Journal of Materials Chemistry C

Accepted Manuscript

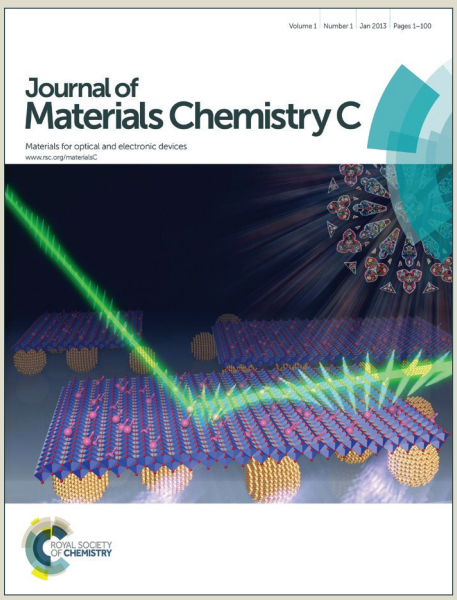

ROYAL SOCIETY OF CHEMISTRY

www.rsc.org/materialsC

Journal Name

ARTICLE

Tuning the Polarity and Surface Activity of Hydroxythiazoles – Extending Applicability of Highly Fluorescent Self-Assembling Chromophores to Supra-Molecular Photonic Structures†

Received 00th January 20xx,
Accepted 00th January 20xx

DOI: 10.1039/x0xx00000x

www.rsc.org/

S. H. Habenicht,[a] S. Schramm,[a] S. Fischer,[b] T. Sachse,[b] F. Herrmann-Westendorf,[b] A. Bellmann,[ac] B. Dietzek,[bd] M. Presselt,*[bd] D. Weiß,[a] R. Beckert,*[a] and H. Görls[e]

A small library of *N*,*N*-diethyl- and -diethanolsulfonamides of differently substituted 2-(2-pyridyl)- and 2-pyrazinyl-4-alkoxythiazoles has been synthesized and investigated in terms of their photophysical properties, electronic structure (quantum chemical calculations at the CAM-B3LYP/6-31+G(d,p) level of theory) and thin film morphology (Langmuir-Blodgett- and spin-cast films). By using the Langmuir-Blodgett technique we show how to exert direct control over the degree of aggregation in thin films made from different thiazole type dyes. In combination with spectroscopic investigations, we gained an in-depth understanding of the influence of aggregation on the electro optical properties of thin films made of the here investigated substances.

Introduction

The 4-hydroxy-1,3-thiazole chromophore and fluorophore is structurally very similar to the naturally occurring firefly luciferin, thus possessing remarkable spectroscopic characteristics.[1, 2] The classical heterocyclic hydroxythiazole core was described by Chabrier *et al.* in 1949,[3] although the thiazolin-4-one structure, the keto-tautomer of the hydroxythiazole, had been proposed at that time and was later proven to be the enol form.[4] In the following years, 4-hydroxy-1,3-thiazoles have been tested for only few applications in biochemistry, e.g. as inhibitors for several enzymes such as cyclooxygenase, 5-lipoxygenase and cyclin-dependent kinase 5.[4-6] During this period, their ability to fluoresce upon photoexcitation was never mentioned. Since the revival of intense scientific investigation on this substance class in 2007,[1] several applications of its derivatives have been developed. Very recently a new derivative has been utilized as a reporter molecule for fluorescence and mass spectrometric detection of a model protein.[7] Furthermore, they have been reported to be fast and specific systems for fluoride ion detection.[8] Recent research indicates that thiazole-based fluorophores, due to their matching excitation and emission characteristics, are potential sensitizers for the highly efficient chemiluminescence of the 2-coumaranones.[9-11] 4-Hydroxythiazole derivatives have furthermore been employed as light-harvesting ligands in Ru^{II} polypyridyl complexes.[12] Thanks to their easy functionalization and tunable optical properties they have been successfully incorporated as blue-emitting species in polymer backbones,[13, 14] as a Förster resonance energy transfer (FRET) energy donor in a terpolymer alongside a Ru^{II} complex as the acceptor unit,[15] and as chromophores in donor-π-acceptor (D-π-A) dyes in dye-sensitized solar cells (DSSCs).[16] It was shown that in DSSCs aggregation of thiazoles reduces the DSSCs performance.[16]
Recent approaches to avoid dye aggregation by introduction of atomic spacers and side chains yielded dramatically increased DSSC efficiencies.[17-21] Beyond this already successful approach of aggregation inhibition, different methods of directed self assembly and aggregation, such as the formation of hydrogen bonds and/or π-π-stacking interactions have shown to be promising approaches for improving the efficiency of optoelectronic and photovoltaic devices.[22-27]
We aim for controlling the formation of supramolecular architectures to be used in photon conversion.[28-33] For this purpose, we utilize self-assembly of amphiphilic molecules, especially at interfaces.[34-41] In the present study we developed amphiphilic hydroxythiazole derivatives by attaching both hydrophilic groups and non-polar chains to the fluorophore: a series of *N*,*N*-dialkylsulfonamide substituted 4-alkoxy-1,3-thiazoles has been synthesized. These compounds can be tuned in their hydrophilicity, which generally opens up opportunities for novel applications, e.g. in biomedicine[42-44] or pharmacy.[45-47]

[a] Institute of Organic Chemistry and Macromolecular Chemistry, Friedrich-Schiller-University, Humboldtstr. 10, 07743 Jena, Germany.
[b] Institute of Physical Chemistry, Abbe Center of Photonics, Friedrich-Schiller-University, Helmholtzweg 4, 07743 Jena, Germany.
[c] Leibniz Institute for Catalysis, Albert-Einstein-Straße 29A, 18059 Rostock, Germany.
[d] Leibniz Institute of Photonic Technology (IPHT), Albert-Einstein-Str. 9, 07745 Jena, Germany.
[e] Institute of Inorganic and Analytical Chemistry, Friedrich-Schiller-University, Humboldtstr. 8, 07743 Jena, Germany.

† Electronic Supplementary Information (ESI) available: Synthetic procedures, additional crystal structure graphics, UV/Vis and fluorescence spectra, XYZ data, further LB isotherms, technical details and ^{1}H NMR spectra. See DOI: 10.1039/x0xx00000x

The new compounds bear either a 2-pyridyl- or a pyrazinyl-substituent in 2-position, different alkoxy groups in 4-position and a *p*-sulfonamide substituted phenyl ring in 5-position. Both *N*,*N*-diethyl- and *N*,*N*-diethanolsulfonamide derivatives have been prepared from each building block. 2-Pyridyl-substituents in 2-position facilitate high quantum yields,[1] pyrazinyl rings were introduced to manipulate electronic features of the compounds.[48] In this paper we present both the synthesis as well as the characterization of the novel thiazoles with a particular focus on the spectroscopic properties and possible surface activity. Photophysical properties of the new sulfonamide containing fluorophores are supplemented by quantum chemical studies.

Results and Discussion

Synthesis

Preparation of the starting material **1** followed a straightforward synthesis based on *Hantzsch* cyclization between 2-bromo-2-phenylethylacetate and pyridine-2-carbothioamide. Synthetic procedures can be found in the literature.[8, 12, 15] The *O*-alkylated derivatives **2a-c** were obtained in very good yields by simple *Williamson* type etherification. They were then treated with neat chlorosulfonic acid in order to obtain the sulfochlorides **3a-c** (84-91% yield). If the reaction was carried out in chloroform, no conversion of the starting materials was observed. The reaction of **3a-c** with diethylamine or diethanolamine yielded new sulfonamides **4a-c** and **5a-c**, respectively, in 77-89% yield (Scheme 1, top). Derivatives **4a** and **5a**, both of which are bearing a methyl ester function, can be further transformed to the corresponding carboxylic acids **6**, **7** (Scheme 1, bottom). Saponification was performed with KOH in aqueous ethanol and the corresponding carboxylic acid was precipitated with dilute HCl. **6** and **7** are soluble in alkaline aqueous solutions.

Compounds that are structurally similar to **4-7** but bearing a pyrazine ring in 2-position of the thiazole were prepared following the same synthetic procedures as applied to obtain **4-7**. A synthetic protocol for the preparation of the starting material **8** (see Scheme **1**, middle) can be found in the literature.[48] Hydroxythiazole **8** was subsequently alkylated with methyl bromoacetate, 1-bromo-3-chloropropane or methyl iodide to obtain the ethers **9a-c**. Chlorosulfonation of **9** and treatment with diethylamine or diethanolamine afforded the sulfonamides **11a-c** and **12a-c** in good to very good yields (Scheme 1, middle). The methyl ester in both **11a** and **12a** were cleaved to **13**,**14** using KOH in aqueous ethanol (Scheme 1, bottom), analogous to the preparation of **6** and **7**.

Chemical structures of the new compounds were confirmed by means of NMR, MS, high resolution MS and UV/Vis spectra. Sulfochlorides **3a-c** and **10a-c** have only been characterized by NMR and MS and were rapidly converted to the corresponding sulfonamides, as they were highly sensitive to humidity. Even if stored in a closed flask in the freezer overnight, isolated yields decreased significantly. It is also noteworthy that none of the sulfochlorides exhibited fluorescence emission, neither in

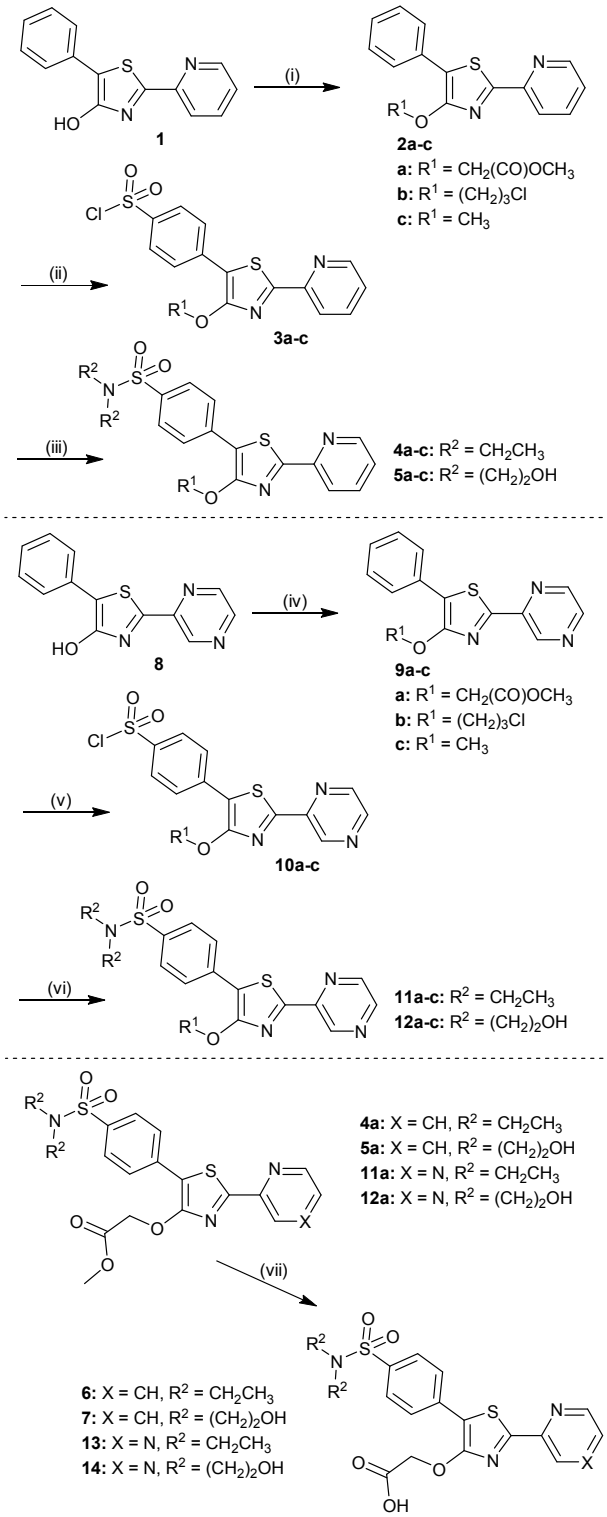

Scheme 1 Top: Synthesis of sulfonamides **4a-c**, **5a-c**. (i) 2a,b: R^1-Br, K_2CO_3, acetone, reflux, 88-94%; 2c: CH_3I, K_2CO_3, acetone, reflux, 91%; (ii) HSO_3Cl, 0 °C - r.t., 84-91%; (iii) $HN(R^2)_2$, NEt_3, CH_2Cl_2, 77-89%. Middle: Synthesis of sulfonamides **11a-c**, **12a-c**. (vi) 9a,b: R^1-Br, K_2CO_3, acetone, reflux, 85-94%; 9c: CH_3I, K_2CO_3, acetone, reflux, 90%; (ii) HSO_3Cl, 0 °C - r.t., 51-85%; (iii) $HN(R^2)_2$, NEt_3, CH_2Cl_2, 30-92%, Bottom: Synthesis of carboxylic acids **6**,**7** and **13**,**14**. (vii) 1. KOH, EtOH, H_2O; 2. HCl. (dil.), 84-97 %.

solution nor in the solid state, most likely due to intersystem crossing to the triplet manifold *via* spin-orbit-coupling.[49-51] The contrary is the case for alkoxy thiazoles **2a-c** and **9a-c**, the corresponding sulfonamides **4a-c**, **5a-c**, **11a-c**, **12a-c** and carboxylic acids **6**, **7**, **13** and **14**. All of these show fluorescence both in the solid state and in solution (*vide infra*), although containing one or more sulfur atoms each, which can promote intersystem crossing to the triplet manifold as mentioned above.

X-Ray Crystal Structures

X-ray crystallographic analysis was performed to confirm successful synthesis of the target compounds, to characterize the molecular geometry, as well as to investigate intermolecular interactions. Single crystals suitable for X-ray structure analysis were obtained from slow diffusion of pentane into a saturated solution of **4c** in EtOAc. The crystal structure of **4c** is depicted in Figure 1. It reveals the almost planar arrangement of the compound. The torsion angles between the three aromatic rings are 3.6(2)° (C4-C5-C6-N2) and 7.8(2)° (C7-C8-C9-C14). The methoxy group is twisted only 6.68(19)° out of plane (C15-O1-C7-N2). While S2 is in plane with the aromatic ring it is attached to (S2-C12-C13-C14: 178.42(11)°), the sulfonamide-nitrogen N3 is distinctly tilted towards the phenyl ring (N3-S2-C12: 109.17(6)°). A look at the molecular packaging of **4c** reveals that the molecules are not arranged parallely due to the steric demand of the ethyl groups on the sulfonamide moiety. Therefore no π-stacking is present in the single crystals. Instead, the molecules are arranged in zigzag like stacks where the orientation of the molecule is alternating. The distance between two similar atoms in parallelly arranged molecules is 8.2(6) Å (see also: Fig.S1-S3, ESI), indicating no π-π-stacking interactions in the crystalline state.[52, 53]

Single Crystals of **11a** that were suitable for X-ray structure analysis were obtained by slow evaporation of a concentrated solution of **11a** in EtOAc. The crystal structure is depicted in Figure 2. Expectedly, the three aromatic rings form a co-planar structure. The pyrazine ring in 2-position of the thiazole core is twisted 2.17(2)° out of plane (N1-C1-C17-N4: 177.83(12)°) and the sulfonamide containing phenyl ring is twisted 7.51(2)° (C2-C3-C4-C5: 172.49(14)°) with regard to the center ring. The glycolic ester moiety is also in plane with the aromatic fluorophore system (C1-N1-C2-O3: 178.81(11)°, C2-O3-C14-C15: 177.90(11)°, C16-O5-C15-C14: -178.33(12)°, C16-O5-C15-O4: 2.7(2)°). Only the sulfonamide moiety, due to the sp^3 hybridised S2, is significantly tilted towards the phenyl ring in 5-position of the thiazole (N2-S2-C7: 107.78(6)°). In the crystal, the molecules are arranged in stacks where the thiazole cores are located on top of one another and the pyrazine ring of one molecule slightly overlaps with the phenyl ring of another (Fig. S4, ESI). The sulfonamide moieties are tilted towards the next molecule in the stack. The distance between the thiazole cores in the different layers is 3.3(3) Å (see Figure 2), thus indicating π-π-stacking interactions in the crystalline state,[52, 53] probably occurring due to the minimization of the overall dipole moment through anti-aligned dipoles.[54, 55]

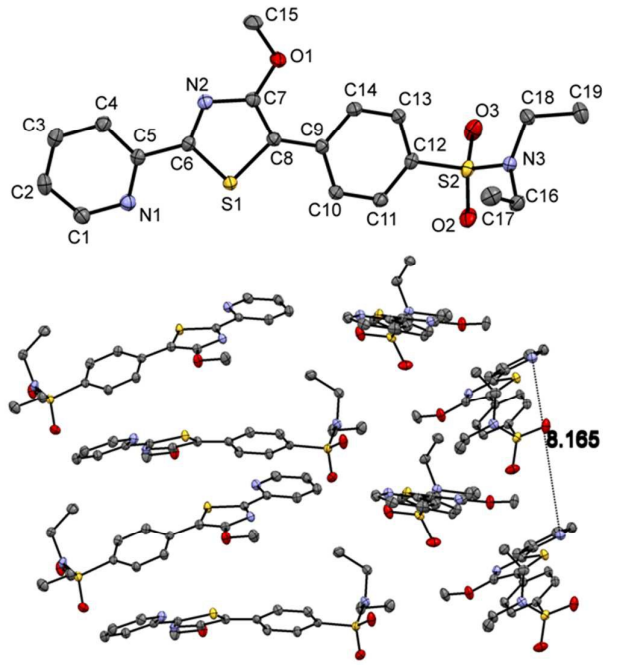

Figure 1 ORTEP plot (50% probability ellipsoids) of **4c**. The numbering scheme (top) and molecular packing (bottom) are shown. Hydrogen atoms were omitted for clarity.

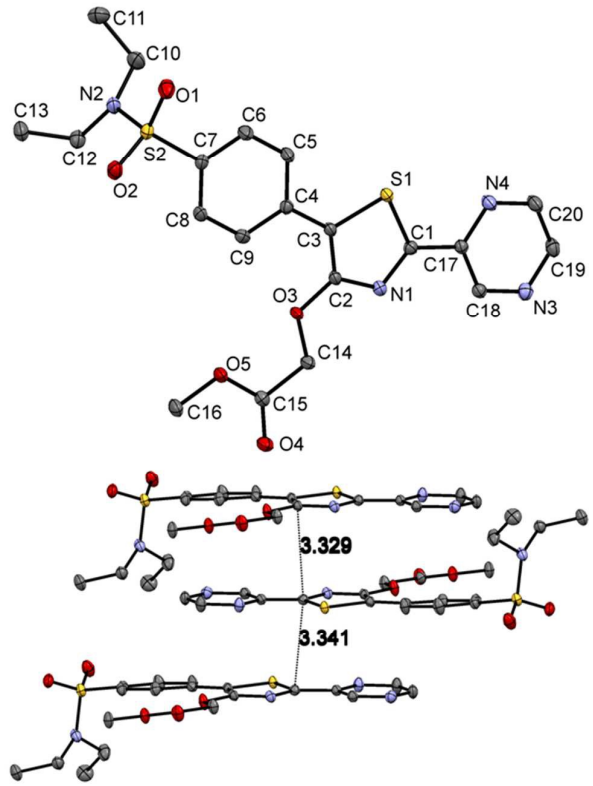

Figure 2 ORTEP plot (50% probability ellipsoids) of **11a**. The numbering scheme (top) and molecular packing (bottom) are shown. Hydrogen atoms were omitted for clarity.

Optical Properties

Spectroscopic data (UV/Vis and fluorescence) for **2a-c**, **4a-c**, **6** and **7** are summarized in Table 1. Since all UV/Vis spectra look very similar, only one example (**6**) is shown in Figure 3. The same is the case for fluorescence emission spectra. All other spectra can be found in the ESI (Fig. S5-S14).

The absorption spectra of all compounds exhibit a single structureless band with maxima between 372 and 378 nm, which can be assigned to $S_0 \rightarrow S_1$ transitions. Values for ε range from 2.05 to 3.02 × 10^4 M^{-1} cm^{-1}. A second, shorter-wavelength absorption band was observed for **2a-c**, **4a-c** and **6**. Only in **2a**, **4a** and **6** those bands were distinctly separate and their maxima are 270, 284 and 285 nm, respectively. They can be assigned to $S_0 \rightarrow S_2$ transitions. The emission maxima range from 440 to 447 nm. Stokes shifts are very similar for all compounds and range from 4084 to 4287 cm^{-1} (0.50-0.53 eV). This is in good agreement with previous observations for similar compounds.[12,15] The fluorescence quantum yields of **2a-c** are 0.85, 0.81 and 0.75, respectively, i.e. they decrease from **2a** to **2c**. No such trend was observed for diethyl sulfonamides **4a-c** (Φ_F = 0.80-0.83) and diethanol sulfonamides **5a-c** (Φ_F = 0.77-0.79). Quantum yields for carboxylic acids **6** and **7** are 0.75 and 0.71, respectively and are therefore slightly lower than all others. Overall it can be said that good to very good quantum yields were achieved for **2a**-**7**. It is also worth mentioning, that the introduction of sulfonamide moieties did not significantly decrease fluorescence quantum yields.

Spectroscopic data (UV/Vis and fluorescence) for **9a-c** and **11a-14** are summarized in Table 1. The absorption spectra of all compounds exhibit a single structureless band with maxima between 385 and 391 nm, which can be assigned to $S_0 \rightarrow S_1$ transitions. Values for ε range from 2.15 to 2.85 × 10^4 M^{-1} cm^{-1}. A second, shorter-wavelength absorption band was observed for all pyrazine derivatives. It can be assigned to $S_0 \rightarrow S_2$ transitions. The maxima range from 274 to 277 nm for **9a-c** and from 286 to 289 nm for **11a-14** (see ESI). All compounds **9a-14** exhibit two emission maxima between 453 and 470 nm. It is noteworthy that for the esters **9a**, **11a** and **12a**, the shorter-wavelength emission band is

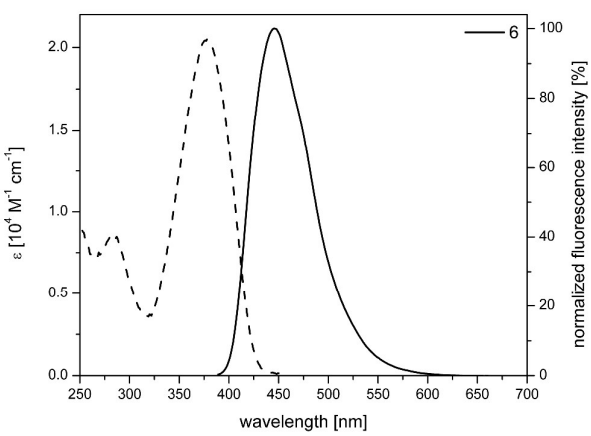

Figure 3 UV/Vis absorption (dashed) and fluorescence emission (solid) spectra of **6**, 2×10^{-6} M in THF.

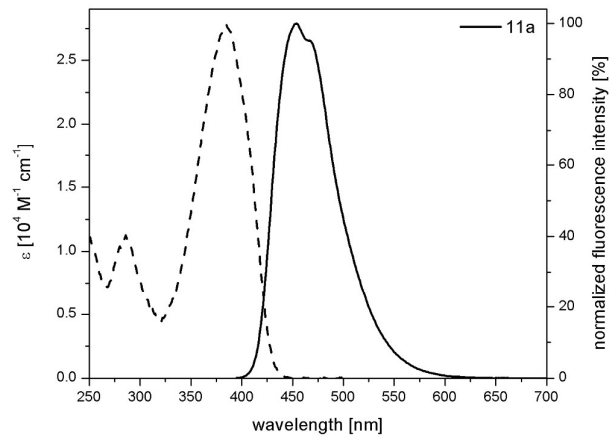

Figure 4 UV/Vis absorption (dashed) and fluorescence emission (solid) spectra of **11a**, 2×10^{-6} M in THF.

slightly more intense than the longer wavelength signal. The opposite is the case for **9b,c**, **11b,c**, **12b,c**, **13** and **14**. The UV/Vis absorption and fluorescence emission spectra of **11a** are depicted in Figure 4. All other spectra can be found in the ESI (Fig. S15-S23). Stokes Shifts are between 3899 and 4654 cm^{-1} (0.48-0.58 eV). Fluorescence quantum yields are very similar for **9a-12c**: they range from 0.72-0.79. Only the carboxylic acids **13** and **14** feature a slightly lower quantum yield of 0.67. As for the pyridyl derivatives, good fluorescence quantum yields were achieved for the pyrazine compounds. The introduction of sulfonamide moieties did not significantly decrease quantum yields and only those of carboxylic acids are slightly lower than all others.

Electronic Structure Calculations

To gain a more detailed insight in the emission and absorption properties of the here presented sulfonamide substituted 4-alkoxy-1,3-thiazoles, we applied density functional theory (DFT) and time dependent density functional theory (TD-DFT) to those derivatives of interest (**4a-c**, **5a-c**, **6**, **7**, **11a-c**, **12a-c**, **13**, **14**). The effect of solvatation (THF) was addressed by means of the polarizable continuum model[56] as implemented in Gaussian 09.[57]

The frontier orbitals of **4a** and **11a** are depicted in Figure 5 as illustrative examples. Both HOMOs and LUMOs are mainly delocalized over the whole molecule with exception of the glycolic ether in 4-position of the thiazole core and the ethyl groups of the sulfonamides. Therefore the MO constructs suggest a significant overlap of the HOMO and the LUMO for the molecules. This observation nicely corresponds with the high experimental extinction coefficients and is also reflected in high theoretical oscillator strengths (*vide infra*) and their highly efficient fluorescence.

Moreover Figure 5 clearly shows that the HOMO- and LUMO-shapes of both compounds **4a** and **11a** are virtually identic. Considering that all calculated absorption and emission properties are only involving these frontier orbitals, this may serve as a possible explanation for the quite small gap between the absorption and emission maxima of pyridyl and

Journal Name

ARTICLE

Table 1 Absorption and emission properties of **2a-c**, **4a-7**, **9a-d** and **11a-14** in THF at room temperature.

entry	$\lambda_{max,abs.}$ [nm]	ε [10^4 M^{-1} cm^{-1}]	$\lambda_{max,em.}$ [nm]	ν_{St} [eV]	ν_{St} [cm^{-1}]	Φ_F
2a	372	2.07	440	0.52	4155	0.85
2b	373	2.31	444	0.53	4287	0.81
2c	374	2.70	444	0.52	4215	0.75
4a	374	2.89	443	0.52	4165	0.83
4b	377	2.63	447	0.52	4154	0.81
4c	378	3.02	447	0.51	4084	0.80
5a	373	2.10	443	0.53	4237	0.78
5b	377	2.89	447	0.52	4154	0.77
5c	377	2.30	448	0.52	4204	0.79
6	378	2.05	446	0.50	4033	0.75
7	377	2.42	446	0.51	4103	0.71
9a	385	2.27	455	0.50	3996	0.76
9b	387	2.15	472	0.58	4654	0.74
9c	387	2.21	471	0.57	4609	0.72
11a	385	2.78	454	0.49	3948	0.79
11b	389	2.74	470	0.55	4430	0.73
11c	390	2.85	470	0.54	4364	0.75
12a	385	2.31	453	0.48	3899	0.77
12b	389	2.55	470	0.55	4430	0.76
12c	389	2.81	470	0.55	4430	0.75
13	391	2.46	468	0.52	4207	0.67
14	389	2.15	467	0.53	4294	0.67

All measurements were performed at r.t. Quinine sulfate was used as standard for the determination of quantum yields (Φ = 0.52).

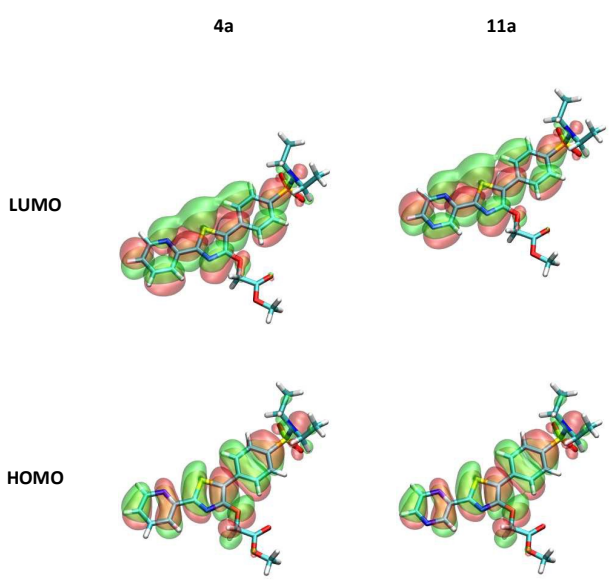

Figure 5 Fontier Orbitals (HOMO, LUMO) of 4a and 11a, optimized at the CAM-B3LYP/6-31+G(d,p) level of theory.

pyrazinyl derivatives (see Table 3).

The calculated absorption and emission maxima are in a good agreement with the experimental values. Nonetheless, it must be said that the calculated absorption wavelengths entail a larger error (0.19–0.29 eV) than the calculated emission wavelengths (0.03–0.11 eV). Yet the error is always within the 0.3 eV margin that is typical for TD-DFT calculations[58, 59] and especially for thiazole-based chromophores like firefly oxyluciferin.[60]

The UV/Vis-absorption as well as the emission properties of the studied molecules only consists of transitions from the HOMO to the LUMO (or *vice versa*). It is noteworthy that all of the here studied derivatives feature very high oscillator strengths for their $S_0 \rightarrow S_1$ transition (0.9180 - 0.9906).

As can be seen in Table 3, the Stokes shifts for all sulfonamide compound can also be calculated within a reasonable margin of error (0.14 – 0.20 eV). All theoretical Stokes shifts are overestimating the experimental value by a mean of 0.16 eV. Since this offset has a very low standard deviation (0.02 eV), the calculated Stokes shift can be corrected by the empirical value of 0.16 eV to give a much smaller discrepancy in comparison with the experimentally determined values (-0.03

– 0.04). This procedure may be important considering the *in silico* prognosis of new thiazoles for further research.

Table 2 Calculated absorption and emission properties to/from the S_1 in THF.

entry	E_{theo} [eV]	E_{theo} [nm]	f	ΔE_{Exp} [eV]
Absorption				
4a	3.51	353	0.98	0.20
4b	3.51	354	0.96	0.22
4c	3.48	357	0.98	0.20
5a	3.51	353	0.98	0.19
5b	3.50	354	0.97	0.21
5c	3.48	357	0.98	0.19
6	3.52	352	0.98	0.24
7	3.52	352	0.99	0.23
11a	3.44	361	0.94	0.22
11b	3.43	361	0.91	0.24
11c	3.40	365	0.93	0.22
12a	3.44	360	0.94	0.22
12b	3.43	362	0.92	0.24
12c	3.41	363	0.93	0.23
13	3.45	360	0.94	0.28
14	3.45	359	0.95	0.26
Emission				
4a	2.85	435	-	0.05
4b	2.82	440	-	0.04
4c	2.81	442	-	0.03
5a	2.85	435	-	0.05
5b	2.82	440	-	0.05
5c	2.81	441	-	0.04
6	2.85	435	-	0.07
7	2.86	434	-	0.08
11a	2.76	449	-	0.03
11b	2.72	456	-	0.08
11c	2.71	458	-	0.07
12a	2.77	448	-	0.03
12b	2.73	455	-	0.09
12c	2.72	457	-	0.08
13	2.76	449	-	0.11
14	2.77	448	-	0.11

All transitions H→L, absorption and emission energies (E_{theo}); oscillator strengths (f), error of the calc. to the exp. value (ΔE_{Exp}), H = HOMO, L = LUMO.

Table 3 Calculated Stokes shifts from the Absoption to the Emission of S^1 in THF.

entry	$E_{Theo\ Stokes}$ [eV]	$\Delta E_{Exp\ Stokes}$ [eV]	$\Delta E_{Exp\ Stokes\ corr.}$ [eV]
4a	-0.66	0.14	-0.02
4b	-0.69	0.17	0.01
4c	-0.67	0.16	0.00
5a	-0.66	0.13	-0.03
5b	-0.68	0.16	0.00
5c	-0.66	0.14	-0.01
6	-0.67	0.17	0.01
7	-0.66	0.15	-0.01
11a	-0.68	0.19	0.03
11b	-0.71	0.16	0.00
11c	-0.69	0.15	-0.01
12a	-0.68	0.20	0.04
12b	-0.70	0.15	-0.01
12c	-0.70	0.15	-0.01
13	-0.69	0.17	0.01
14	-0.68	0.15	-0.01

Stokes shift energies ($E_{Theo\ Stokes}$); error of the calc. to the exp. value ($\Delta E_{Exp\ Stokes}$), error of the corrected calc. to the exp. value ($\Delta E_{Exp\ Stokes\ corr}$).

Solubility and Surface Activity

To utilize the amphiphilicity of the thiazoles and the resulting self-assembly at the air-water interface we applied the Langmuir-Blodgett (LB) technique for assembling and deposition of the dyes.[36, 61-64] For this purpose the thiazoles were dissolved in a volatile solvent (typically chloroform), the resulting solution was carefully dispersed on the water surface of the LB-trough and the LB-experiments were started after solvent evaporation. The LB-isotherms of **4a-c**, **5a-c**, **6**, **7**, **11a-c**, **12a-c**, **13** and **14** were recorded at a constant compression speed of 375 mm^2/min. Under these conditions the compounds **6**, **12c** and **13** did not show any resistance to compression on the LB-trough which suggests that they are getting dissolved in the water subphase. Substance **14** is not soluble in organic solvents and was therefore not tested, thus we are discussing only the derivatives of types **4**, **5**, **11** and **12** in the following.

Figure 6 depicts the isotherms of **4a-c** and **11a-c**. The isotherms of **5a-c**, **7** and **12a,b** can be found in the ESI (Fig. S24). The corresponding values for collapse area (A_c) and pressures (π_c) are shown in Table 4. The collapsing point here is defined as the inflexion point of the isotherm[39] that is generated by a pressure-induced phase- transition.[65] The third parameter that is considered to compare the isotherms to each other is A_{ext}, which is the hypothetical area per molecule of the liquid phase at a surface pressure of 0 mN/m (see Figure 6). An exemplary fit of the linear region of the graph that was used for the determination of A_{ext} is depicted in Figure 6 for **4b**.

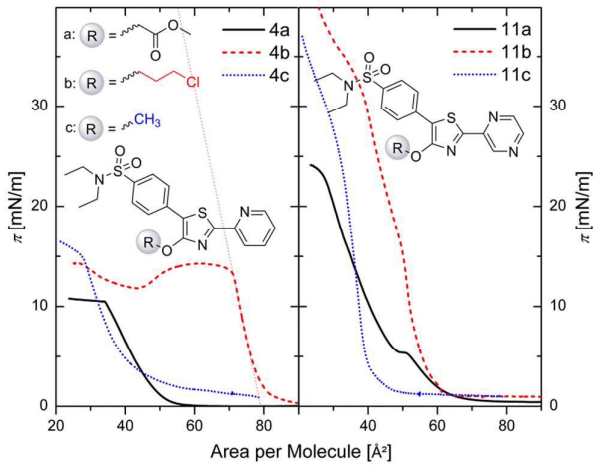

Figure 6 LB-isotherms of **4a-c** and **11a-c**, recorded with a constant barrier speed of 5 mm/min. For the measurement a volume of 50µL was spread on the trough (concentrations are presented in Table 4). An exemplary linear fit is shown for **4b**.

The isotherms of **5a-c**, **7**, **12a** and **b** exhibit an almost linear curve progression at high surface-pressure and no signs of phase transition (Figure 6). Moreover, their A_{ext} value is already very low before the compression starts (around 25 Å^2). The same LB-behavior is found for Lauric acid and is explained by its slight solubility in water.[61] We therefore assume that **5a-c**, **7**, and **12a,b** are also slightly water soluble. This seems reasonable due to the two hydroxyl-groups on the sulfonamide moiety which increase the hydrophilic properties.

4a-c show a sharp collapse-point at relatively low pressures (12 - 15 mN/m, see Figure 6 and Table 4). This indicates a typical phase-transition as observed for many long-chain amphiphiles.[61] As opposed to **4a-c**, isotherms of **11a-c** show several weak points of inflection, particularly **11b**, and their collapse pressures are significantly and systematically higher, while the only molecular structural difference to **4** is the replacement of the pyridyl moiety by the pyrazinyl ring.

A very dense packing in the Langmuir monolayers in the trough is observed for derivatives **5**, **7**, **12** that have alcohols attached to the sulfonamide group to make it even more polar. Thus the polar heads provide a strong hydrophilic anchor, which causes small molecular areas in the dense Langmuir films of about 20 Å² as shown in Table 4. In contrast, derivatives of types **4** and **11**, which are bearing short alkyl chains instead of alcohols attached to the sulfonamide, are showing significantly larger molecular areas ranging from 40 to 70 Å² because of the weaker hydrophilic anchor. Additionally, the molecular areas of **4a-c** and **11a-c** depend on the substituents introduced at the 4-hydroxy-group of the thiazole. Expectedly, a- and b-type substitutions induce stronger interactions of the chromophores with the subphase as compared to the methyl-(c)-substitution, thus causing generally somehow larger molecular areas. Remarkably, the molecular area of 4b is exceptionally large (A_c = 70 Å^2 and A_{ext} = 74 Å^2) and indicates a flat orientation of **4** at the water surface (largest molecular spatial demand on a flat surface approximately 5 Å × 14 Å ≈ 70Å²).

Table 4 Concentrations of the spread solutions and calculated collapse parameters of the LB-isotherms.

substance	c [mmol/l]	π_c [mN/m]	A_c [Å²]	A_{ext} [Å ²]
4a	2.17	12	33	44
4b	2.15	14	70	74
4c	2.48	15	27	42
5a	2.03	-	-	20
5b	2.01	-	-	24
5c	2.30	-	-	18
7	2.09	-	-	18
11a	2.16	23	28	62
11b	2.14	30	30	56
11c	2.47	27	32	40
12a	2.02	-	-	25
12b	2.00	-	-	27

A_{ext}, value of the area per molecule at the theoretical pressure of $\pi = 0$; A_c and π_c, values of the area per molecule and the pressure at the collapse-point of the isotherm.

As discussed qualitatively above, the most obvious polar anchors of the chromophores are the sulfonamide groups highlighted by green ellipsoids in Figure 7. To estimate the possible weight of further polar moieties we computed the electrostatic potential at the van-der-Waals surface as a sum over contributions due to partial charges at every atomic site (see Figure 7). Partial charges have been partitioned using the MMFF94[66] force field after quantum chemical optimizations considering polarizable continuums as artificial environment. In each case, the methyl ester group is pointing away from the rest of the molecule, an unlikely conformation for a single molecule at an air water interface. Instead, the methyl ester group will most likely bend into the water phase. However, possible anchor groups at the interface can clearly be identified by their high polarity in decreasing order of anchoring strength from Figure 7: methyl esters, sulfuryl moieties, hydroxyethyl groups, pyrazinyl and pyridyl rings.

Figure 7 reveals that, additionally to the sulfuryl moiety, the methyl ester and the pyrazinyl/pyridyl rings show considerable polarity. Therefore, **4a** and **11a** appear likely to be anchored with one long side of the chromophore on the water surface, thus explaining the medium sized experimentally determined molecular areas of 44 and 62 Å², respectively. As can be seen in Figure 7, the pyrazinyl ring in **11** exhibits a lower dipole moment making it a slightly worse anchor as compared to the pyridinyl-ring in **4**, thus allowing **11** to leave the flat orientation at lower surface pressures than substances **4**. Considering the fact that substances of type **11** stack well in the solid state (see Figure 2), in contrast to substances **4**, we conclude that substances of type **11** gradually move into an upright orientation as the surface pressure increases. Substances of type **4**, however, cannot stack in such an upright orientation causing the highly ordered structure to break down completely at a certain well-defined surface pressure. Figure S25 (see ESI)

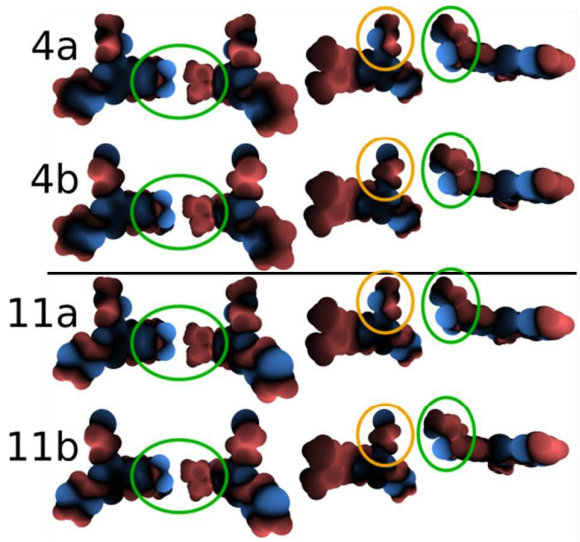

Figure 7 Electrostatic potential on the van-der-Waals surfaces of molecules **4a**, **4b**, **11a** and **11b** (top to bottom) in different orientations (left to right) for geometries optimized at the CAM-B3LYP 6-31+g(d,p) level of theory including solvent effects using the polarizable continuum model. Red, blue and black correspond to a positive, negative and vanishing electrostatic potential, respectively. Green and orange ellipses emphasize the two highly polar groups, namely the sulfonamide and the glycolic ester moieties, respectively.

shows that due to the hydroxy-ethyl groups attached to the sufonamide in **5** and **12**, the sulfonamide gets even more polar and takes precedence, thus supposedly causing upright chromophore orientations.

Morphology and Optical Properties of Langmuir, LB and Spin Cast Films

To find out how the optical properties change with varying LB conditions, Langmuir-Blodgett-films (LB) were deposited on quartz-glass and characterized by means of UV/Vis-spectroscopy, fluorescence-measurements and atomic force microscopy (AFM). Spin-coated (SC) films and solutions were prepared as references. The two compounds **11a** and **11b** were investigated more closely because their LB isotherms differ significantly. Another advantageous feature of these two dyes is their comparatively high collapse-point, which allows varying π over a larger scale.

Employing AFM, we probed the surface morphology of LB- and SC-films of **11a** deposited onto a quartz glass surface to investigate the evenness of the films and the influence of the respective deposition method on film morphology. Height images as well as phase images, which probe the local stiffness of the film surface, are shown for **11a** in Figure 8. The LB and SC films have RMS surface roughnesses of 0.45 and 3.20 nm, respectively. Thus, the surface roughness of the SC film, expectedly, is significantly higher than that of the LB film. This can also be seen in the height images (see Figure 8a,c). A very narrow distribution of the AFM phase angle was observed for the LB film (Figure 8b) while the SC film shows significantly larger phase angles in areas where the surface is especially

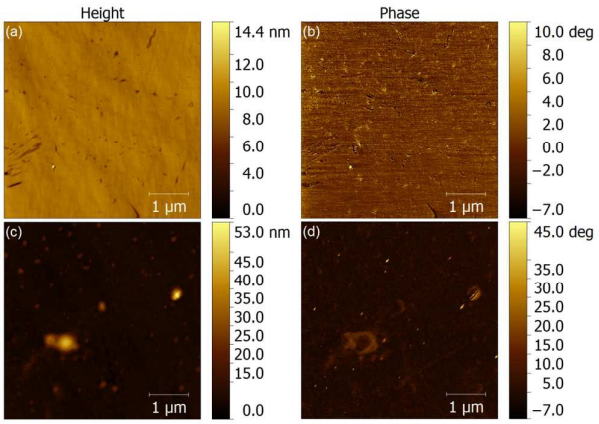

Figure 8 AFM images of LB- (a, b) and SC-films (c, d) of **11a**, deposited on quartz glass (π = 5 mN/m). Individual scale bars are shown to the right of every image.

uneven (Figure 8d). Thus, smooth thin films with rather homogeneous molecular orientation are obtained via the LB-technique whereas spin-casting yields apparently stochastic molecular orientations and cluster formations and shows a significant amount of random substance accumulation.

The absorption spectra of **11a** and **11b** (chloroform solution, LB- and SC-film) are shown in Figure 9 (for the solid state samples the absorbance at the minimum was set to zero). The structureless band which appears at 390 nm in $CHCl_3$ for **11a** and **11b** is red-shifted to 400 nm in the SC films. The LB films of 5 monolayers (ML) have been deposited at very high surface pressure (23 mN/m for **11a** and 28 mN/m for **11b**) and are expected to show a high molecular ordering. As seen from Figure 9 a higher molecular order in the LB-films as compared to the SC-films is revealed by the vibrational progression that is significantly better resolved in the spectra of the LB-films as compared to the SC-films (a simple estimation of the coupling energy in the vibrational progression gives an energy difference of about 1350±100 cm^{-1}). Stochastic molecular orientations, like in the SC-films, are also present in Langmuir-films in the quasi liquid phase at low surface pressures. Thus, the transition from the disordered to the ordered phase can be mimicked by systematically varying the surface pressure at deposition of the Langmuir-films.[61, 67] The corresponding changes in the spectral shapes and vibrational progressions are shown in Figure 10. Interestingly the intensity distribution in the vibrational progression is altered from SC- to LB-films. Hence the potentials of the associated states are altered due to intermolecular interactions.

The dependence of the fluorescence spectra of **11a** and **11b** on the surface pressure was investigated directly for the Langmuir-films on the LB-trough surface by means of a custom-made fluorescence online-monitoring setup. Fluorescence spectra of **11a** that were normalized to the molecular density (same surface concentration) as obtained from the LB-isotherms are depicted in Figure 11. The fluorescence intensities increase with increasing surface

Journal Name

ARTICLE

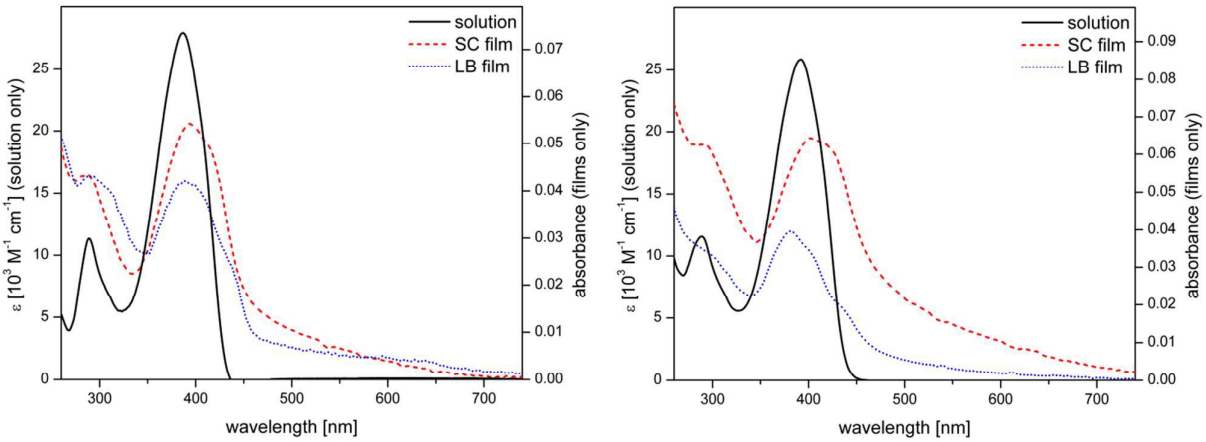

Figure 9 UV/Vis-spectra of **11a** (left) in solution ($CHCl_3$; c= 20 µg/ml), as SC film (c = 2.16×10^{-3} M; 30 rps for 30 s) and as LB film (5 ML; π = 20 mN/m). The intensity of the LB film was increased by factor 4 for clarity. UV/Vis-spectra of **11b** (right) in solution ($CHCl_3$; c= 100 µg/ml), as SC film (c = 2.14×10^{-3} M; 30 rps for 30 s) and as LB film (5 ML; π = 32 mN/m).

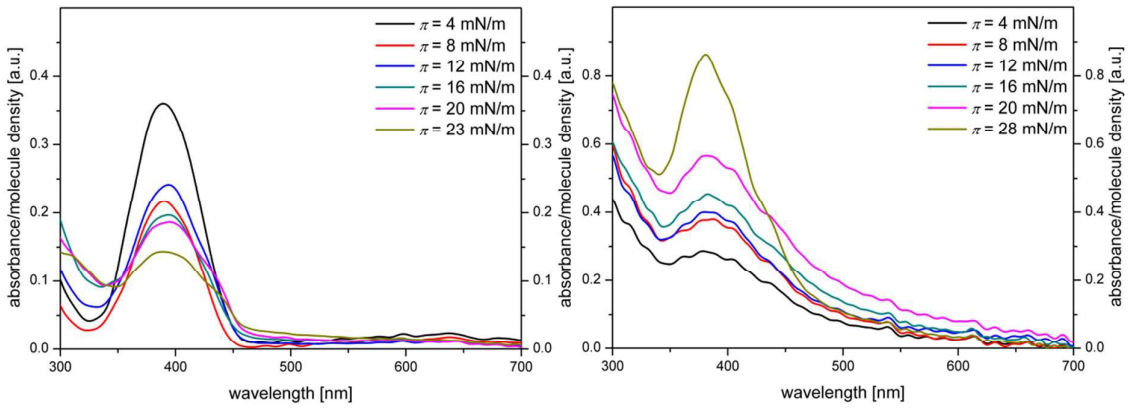

Figure 10 UV/Vis spectra of LB films at different π of **11a** (5mL deposited at 4, 8, 12, 16, 20 and 23 mN/m, top) and **11b** (4, 8, 12, 16, 20 and 28 mN/m, bottom). The spectra have been normalized with regard to the molecule density per surface area.

pressure, which may be explained with a reduced misfit between the irradiation angle of excitation (intermediate incidence) and chromophore orientations. As can be seen from Figure 11, no disctinct change in the spectral shape or wavelength of the fluorescence maximum occurs.

In contrast to **11a,** whose fluorescence intensity is increasing with increasing surface pressure, the fluorescence intensity of **11b** is almost constant when normalized with regard to the molecule density for low pressures (<1 mN/m) as shown in Figure 12. For these low surface pressures the fluorescence spectra become narrower for increasing surface pressures, but the maximum is retained at 460 nm, which is about the same value as found for THF-solutions of **11b** (see Table 2). When further increasing the surface pressure, the shape of the fluorescence spectra changes: the band at 470 nm decreases while a second band at 542 nm almost retains its intensity, finally dominating the fluorescence spectrum at the rather large surface pressure of 27.55 mN/m.

The spectral changes of **11b** with increasing surface pressure can be explained in the following manner: At low surface pressures one can expect stochastically distributed dye molecules without appreciable intermolecular interaction, similar to solutions or amorphous phases. Indeed the optical properties of these LB-films are very similar to those of the dissolved samples. Further increase of the surface pressure is expected to cause alignment of the dyes and possibly

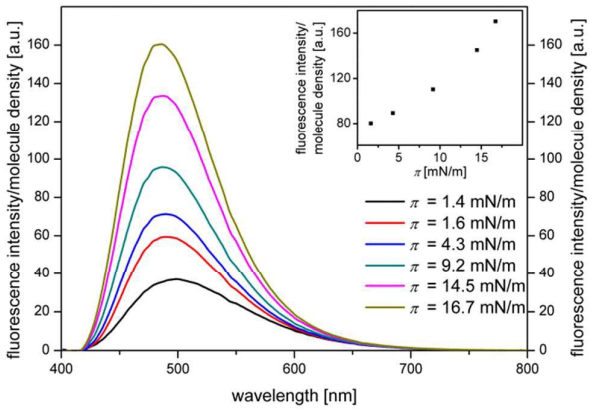

Figure 11 Fluorescence of the Langmuir films of **11a** recorded at different π. The spectra were corrected by subtraction of a spectrum of the empty LB-trough and normalized with regard to the molecule density. Inset: Dependence of corrected fluorescence intensity on π.

formation of H-aggregates that are weakly fluorescent.[68-70] A further possibility for the steady reduction of the fluorescence at 470 nm might by an increasing misfit between the irradiation angle and chromophore orientations. However, the 542 nm-fluorescence that dominates the fluorescence spectrum at high surface pressures at deposition can be clearly assigned to an excimer emission as known from e.g. different perylene derivatives.[71-73] Other groups report similar findings for excimer emission bands in LB-films of pyrene,[74] indocarbocyanine[75] or merocyanine dyes.[76] Furthermore, the absence of a vibrational progression in the fluorescence spectrum supports the assignment to an excimer.

Figure 13 shows that the LB-films produced from **11a** exhibit the same spectral features as their Langmuir-analogues discussed above, except showing no systematic intensity trend, probably due to inhomogenities that arose during the deposition. In case of **11b** all the essential features discussed for the Langmuir-films above are retained after deposition of corresponding LB-films as shown in Figure 13, particularly the intense eximer fluorescence at $\pi = 28$ mN/m. To show the evolution of the excimer band with increasing surface pressure, its intensity relative to the band at 470 nm (*i.e.* I(542 nm)/I(470 nm)) is plotted versus the surface pressure in the inset in Figure 13.

Experimental Section

General Procedures and Molecular Characterization: Reagents were purchased from commercial sources and were used directly unless otherwise stated. All solvents were of reagent grade and were dried according to common practice and distilled prior to use. Reactions were monitored by TLC, which was carried out on 0.2 mm Merck silica gel plates (60 F_{254}). ^{1}H and ^{13}C NMR spectra were recorded on Bruker Avance 250 and 400 spectrometers, chemical shifts (δ) are given relative to signals arising from the solvent. Mass spectra were recorded using a Finnigan MAT SSQ 710. Melting points were determined with a Cambridge Instruments Galen III apparatus (Boëtius system) and are uncorrected.

Langmuir and LB-Films: A KSV NIMA "alternate small" LB-trough with a Wilhelmy balance was employed for the π-A-isotherm measurements as well as the LB film preparations. A chloroform solution (for concentrations see Table 4) of the compound was placed at ambient temperature onto an aqueous subphase of ultrapure water (18 mΩ cm). The solution was spread on the surface with a pipette. In all cases films were compressed after 10 minutes allowing the chloroform to evaporate. The samples and the isotherms were fabricated with a constant compression rate of 375 mm^2/min (barrier speed: 5 mm/min). The deposition of the layers on the quartz glass (30mm × 5mm × 1mm) was done using Y-type dipping (dipping speed: 5 mm/min) and keeping the monolayer under constant pressure. Prior to the transfer, the substrates were treated with chloroform, acetone and iso-propanol in the ultrasonic bath (each solvent 3 times for 10 min). The glass slides were stored under iso-propanol over night in order to make them hydrophilic.

Atomic Force Microscopy: AFM was carried out using a Veeco Digital Instruments Dimension 3100 AFM in tapping mode with a silicon tip (radius < 8 nm) at 300 kHz with a force constant of ≈ 40 N m^{-1} (Budget Sensors Tap 300-G).

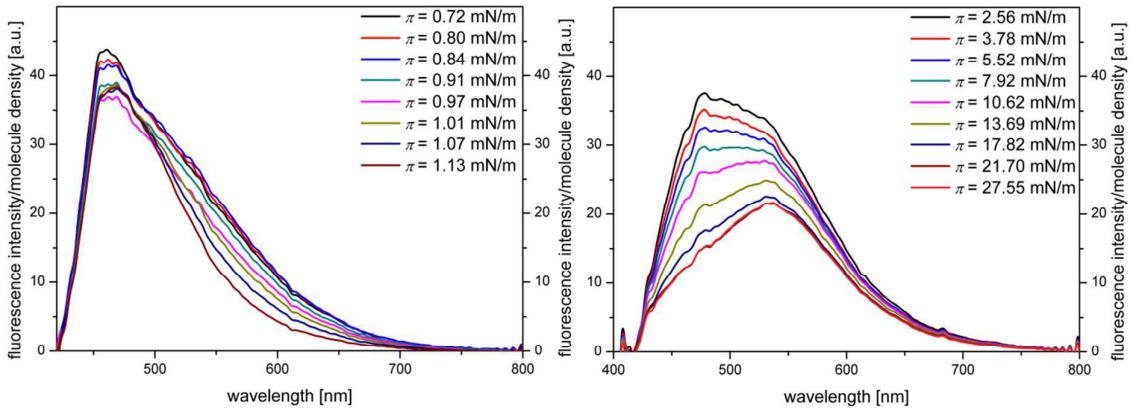

Figure 12 Fluorescence of the Langmuir films (**11b**) for several different π. The spectra were corrected by subtraction of a spectrum of the empty LB-trough and normalized to the molecule density per area.

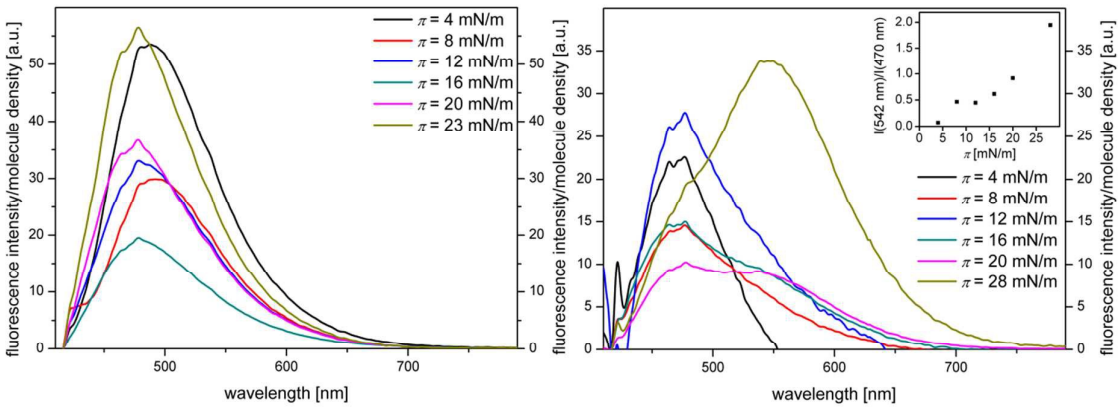

Figure 13 The fluorescence spectra of the LB films deposited at different pressures normalized to the molecule density (left: **11a**; right: **11b**). Inset: Ratio of the fluorescence intensities at 542 and 470 nm at different π.

Spectroscopic Methods: UV/Vis spectra (THF) were recorded with a PerkinElmer LAMBDA 45 UV/Vis spectrometer, emission spectra (THF) were recorded using a JASCO FP-6500 spectrofluorometer. Measurements of the fluorescence intensity were carried out on a PerkinElmer LAMBDA 45 UV/Vis spectrometer and JASCO FP-6500 spectrofluorometer in the perpendicular excitation–emission geometry, while the absorbance at the excitation wavelength used was adjusted to be between 0.04 and 0.05. The calculation of fluorescence quantum yields was done according to the following equation:[77]

$$\Phi = \Phi_r \frac{I}{I_r} \frac{A_r}{A} \frac{n^2}{n_r^2},$$

where Φ is the quantum yield, I is the corrected integrated emission intensity, A is the absorbance at the excitation wavelength and n is the refractive index of the solvent. The subscript r refers to a reference fluorophore of known quantum yield. Here we used quinine sulfate (Φ = 0.52)[78]. All thiazoles were excited as close as possible to their absorption maximum while staying inside the excitation range given in the literature.[79]

Spectroscopic measurements of the compound films: The fluorescence spectra were recorded on a home build setup. This consists of an Isoplane 320 Spectrograph with a cooled Pixis CCD-camera from Princeton Instruments. As excitation sources fiber coupled 5mW laser modules with different wavelength were used. Long pass filters with low self-fluorescence from ITOS were placed in front of the spectrograph to block scattered excitation light. The collected data were afterwards corrected by a self-written Labview program. This removes cosmic rays, filter self-fluorescence and accounts for the setup response function.

Theoretical Methodology: After an initial systematic conformational search with MMFF[66], the best geometries were optimized using at the CAM-B3LYP/6-31+G(d,p)[80, 81] level of theory as implemented in Gaussian 09[57]. Ground state optimization and its validation via frequency calculation were followed by the calculation of the six lowest singlet excited states. This provided insight into the absorption properties of the here presented compounds. Fluorescence emission was calculated according to Kasha[82] from the S_1 equilibrium structure. The effects of solvatation (THF) have been addressed state specific for all calculations of ground and excited states properties by means of the polarizable continuum model[56] as implemented in Gaussian 09.

Synthesis of the compounds: Detailed synthetic procedures can be found in the Supporting Information.

Crystal Structure Determination: The intensity data were collected on a Nonius KappaCCD diffractometer, using graphite-monochromated Mo-Kα radiation. Data were corrected for Lorentz and polarization effects; absorption was taken into account on a semi-empirical basis using multiple-scans.[83-85] The structure was solved by direct methods (SHELXS)[86] and refined by full-matrix least squares techniques against Fo^2 (SHELXL-97)[86]. All hydrogen atoms were located by difference Fourier synthesis and refined isotropically. Mercury (Version 3.3 (Build RC5), Cambridge Crystallographic Data Centre) was used for structure representations.

Crystal Data for **4c** : $C_{19}H_{21}N_3O_3S_2$, Mr = 403.51 gmol^{-1}, yellow prism, size 0.096 x 0.086 x 0.075 mm^3, orthorhombic, space group P n a 2_1, a = 22.1463(3), b = 10.5116(1), c = 8.1653(1) Å, V = 1900.83(4) Å^3 , T= -140 °C, Z = 4, $\rho_{calcd.}$ = 1.410 gcm^{-3}, μ (Mo-K$_\alpha$) = 3.06 cm^{-1}, multi-scan, transmin: 0.6921, transmax: 0.7456, F(000) = 848, 14865 reflections in h(-28/28), k(-13/13), l(-10/10), measured in the range 2.67° $\leq \Theta \leq$ 27.48°, completeness Θ_{max} = 99.7%, 4347 independent reflections, R_{int} = 0.0189, 4276 reflections with $F_o > 4\sigma(F_o)$, 328 parameters, 1 restraints, $R1_{obs}$ = 0.0217, wR^2_{obs} = 0.0588, $R1_{all}$ = 0.0222, wR^2_{all} = 0.0593, GOOF = 1.076, Flack-parameter 0.01(4), largest difference peak and hole: 0.206 / -0.188 e Å^{-3}.

Crystal Data for **11a** : $C_{20}H_{22}N_4O_5S_2$, Mr = 462.54 gmol^{-1}, light_yellow prism, size 0.140 x 0.128 x 0.106 mm^3, triclinic, space group P $\bar{1}$, a = 7.0339(1), b = 12.5011(3), c = 12.5338(3) Å, α = 76.065(1), β = 89.022(1), γ = 75.506(1)°, V = 1034.54(4) Å^3 , T= -140 °C, Z = 2, $\rho_{calcd.}$ = 1.485 gcm^{-3}, μ (Mo-K$_\alpha$) = 2.99 cm^{-1}, multi-scan, transmin: 0.7186, transmax: 0.7456, F(000) = 484, 6495 reflections in h(-9/9), k(-16/16), l(-16/10), measured in the range 1.74° $\leq \Theta \leq$ 27.50°, completeness Θ_{max} = 99%, 4710

independent reflections, R_{int} = 0.0129, 4448 reflections with $F_o > 4\sigma(F_o)$, 368 parameters, 0 restraints, $R1_{obs}$ = 0.0316, wR^2_{obs} = 0.0794, $R1_{all}$ = 0.0339, wR^2_{all} = 0.0817, GOOF = 1.067, largest difference peak and hole: 0.421 / -0.373 e $Å^{-3}$.

Conclusions

The present work describes the synthesis and photophysical properties of novel fluorescent and amphiphilic sulfonamide-substituted hydroxythiazole derivatives. Optical properties of these compounds have been investigated and quantum chemical calculations (CAM-B3LYP/6-31+G(d,p) level of theory) were performed in order to explain the experimental results. Structure-property relationships have emerged from a combination of experimental spectroscopic data and DFT/TDDFT calculations. Absorption and emission properties as well as quantum yields agree nicely with the quantum chemical calculations.

We further we showed how to exert direct control over the degree of aggregation in thin films made of different thiazole type dyes. Upon variation of the different substituents in 2- and 4-position and on the sulfonamide moiety (*i.e.* altering their relative polarity / anchoring strength) the chromophores can be oriented relative to the subphase surface of the LB-trough. In combination with spectroscopic investigations, we gained an in-depth understanding of the influence of aggregation on the electro optical properties of thin films made of the here investigated substances. In-depth investigations to gain detailed information on the molecular packing of our compounds in Langmuir and LB films are currently ongoing. A next step is to perform investigations on active layers or possibly entire devices. Work along these lines is currently in progress and will be reported in due course.

Acknowledgements

The authors thank the Bundesministerium für Wirtschaft und Energie (BMWi KF2258002CS2) and the Bundesministerium für Bildung und Forschung (BMBF FKZ 03EK3507) for financial support. S. F is grateful for financial support from the Deutsche Forschungsgemeinschaft DFG (PR 1415/2). St. S. gratefully acknowledges the Friedrich-Ebert-Stiftung for financial support. T. S. Acknowledges the German Federal Environmental Foundation for his fellowship. Additionally, we thank Dr. W. Günther and G. Sentis for recording the NMR spectra and Mrs. Schönau and Mrs. Heineck for recording the mass spectra.

Notes and references

‡ Crystallographic data deposited at the Cambridge Crystallographic Data Centre under CCDC-1434601 for **4c** , and CCDC-1434602 for **11a** contain the supplementary crystallographic data excluding structure factors; this data can be obtained free of charge via www.ccdc.cam.ac.uk/conts/retrieving.html (or from the Cambridge Crystallographic Data Centre, 12, Union Road, Cambridge CB2 1EZ, UK; fax: (+44) 1223-336-033; or deposit@ccdc.cam.ac.uk).

* To whom correspondence should be addressed: c6bera@uni-jena.de and martin.presselt@uni-jena.de

1 U.-W. Grummt, D. Weiß, E. Birckner and R. Beckert, Pyridylthiazoles: Highly Luminescent Heterocyclic Compounds, *J. Phys. Chem. A*, 2007, **111**, 1104–1110.
2 E. Täuscher, D. Weiß, R. Beckert, J. Fabian, A. Assumpção and H. Görls: Classical heterocycles with surprising properties: the 4-hydroxy-1,3-thiazoles, *Tetrahedron Lett.*, 2011, **52**, 2292-2294.
3 P. Chabrier, S. H. Renard and K. Smarzewska: Sur les composes organiques soufres. II., *Bull. Soc. Chim. France*, 1949, 237.
4 F. A. J. Kerdesky, J. H. Holms, J. L. Moore, R. L. Bell, R. D. Dyer, G. W. Carter and D. W. Brooks: 4-Hydroxythiazole inhibitors of 5-lipoxygenase, *J. Med. Chem.*, 1991, **34**, 2158-2165.
5 F. A. J. Kerdesky, C. D. W. Brooks, K. I. Hulkower, J. B. Bouska and R. L. Bell: Conversion of cyclooxygenase inhibitors into hydroxythiazole 5-lipoxygenase inhibitors, *Bioorg. Med. Chem.*, 1997, **5**, 393-396.
6 R. M. Rzasa, M. R. Kaller, G. Liu, E. Magal, T. T. Nguyen, T. D. Osslund, D. Powers, V. J. Santora, V. N. Viswanadhan, H.-L. Wang, X. Xiong, W. Zhong and M. H. Norman: Structure–activity relationships of 3,4-dihydro-1*H*-quinazolin-2-one derivatives as potential CDK5 inhibitors, *Bioorg. Med. Chem.*, 2007, **15**, 6574-6595.
7 S. Wolfram, H. Wurfel, S. H. Habenicht, C. Lembke, P. Richter, E. Birckner, R. Beckert and G. Pohnert: A small azide-modified thiazole-based reporter molecule for fluorescence and mass spectrometric detection, *Beilstein J. Org. Chem.*, 2014, **10**, 2470-2479.
8 L. K. Calderón-Ortiz, E. Täuscher, E. Leite Bastos, H. Görls, D. Weiß and R. Beckert: Hydroxythiazole-Based Fluorescent Probes for Fluoride Ion Detection, *Eur. J. Org. Chem.*, 2012, **2012**, 2535-2541.
9 L. F. M. L. Ciscato, F. H. Bartoloni, A. S. Colavite, D. Weiss, R. Beckert and S. Schramm: Evidence supporting a 1,2-dioxetanone as an intermediate in the benzofuran-2(3H)-one chemiluminescence, *Photochem. Photobiol. Sci.*, 2014, **13**, 32-37.
10 S. Schramm, D. Weiß, H. Brandl, R. Beckert, H. Görls, D. Roca-Sanjuán, I. Navizet, Investigations on the synthesis and chemiluminescence of novel 2-coumaranones, *ARKIVOC*, 2013, **3**, 174-188.
11 S. Schramm, L. F. M. L. Ciscato, P. Oesau, R. Krieg, J. F. Richter, I. Navizet, D. Roca-Sanjuán, Investigations on the synthesis and chemiluminescence of novel 2-coumaranones - II, D. Weiß, R. Beckert, *ARKIVOC*, 2015, **5**, 44-59.
12 R. Menzel, E. Täuscher, D. Weiß, R. Beckert and H. Görls: The Combination of 4-Hydroxythiazoles with Azaheterocycles: Efficient Bidentate Ligands for Novel Ruthenium Complexes, *Z. Anorg. Allg. Chem.*, 2010, **636**, 1380-1385.
13 A. M. Breul, C. Pietsch, R. Menzel, J. Schäfer, A. Teichler, M. D. Hager, J. Popp, B. Dietzek, R. Beckert and U. S. Schubert: Blue emitting side-chain pendant 4-hydroxy-1,3-thiazoles in polystyrenes synthesized by RAFT polymerization, *Eur. Polym. J.*, 2012, **48**, 1339-1347.
14 R. Menzel, A. Breul, C. Pietsch, J. Schäfer, C. Friebe, E. Täuscher, D. Weiß, B. Dietzek, J. Popp, R. Beckert and U. S. Schubert: Blue-Emitting Polymers Based on 4-Hydroxythiazoles Incorporated in a Methacrylate Backbone, *Macromol. Chem. Phys.*, 2011, **212**, 840-848.
15 B. Happ, J. Schäfer, R. Menzel, M. D. Hager, A. Winter, J. Popp, R. Beckert, B. Dietzek and U. S. Schubert: Synthesis and Resonance Energy Transfer Study on a Random

Terpolymer Containing a 2-(Pyridine-2-yl)thiazole Donor-Type Ligand and a Luminescent [Ru(bpy)$_2$(2-(triazol-4-yl)pyridine)]$^{2+}$ Chromophore, *Macromolecules*, 2011, **44**, 6277-6287.

16 R. Menzel, D. Ogermann, S. Kupfer, D. Weiß, H. Görls, K. Kleinermanns, L. González and R. Beckert: 4-Methoxy-1,3-thiazole based donor-acceptor dyes: Characterization, X-ray structure, DFT calculations and test as sensitizers for DSSC, *Dyes Pigm.*, 2012, **94**, 512-524.

17 H.-J. Son, C. H. Kim, D. W. Kim, N. C. Jeong, C. Prasittichai, L. Luo, J. Wu, O. K. Farha, M. R. Wasielewski and J. T. Hupp: Post-Assembly Atomic Layer Deposition of Ultrathin Metal-Oxide Coatings Enhances the Performance of an Organic Dye-Sensitized Solar Cell by Suppressing Dye Aggregation, *ACS Appl. Mater. Interfaces*, 2015, **7**, 5150-5159.

18 N. Koumura, Z.-S. Wang, S. Mori, M. Miyashita, E. Suzuki and K. Hara: Alkyl-Functionalized Organic Dyes for Efficient Molecular Photovoltaics, *J. Am. Chem. Soc.*, 2006, **128**, 14256-14257.

19 T. Lei, J.-Y. Wang and J. Pei: Roles of Flexible Chains in Organic Semiconducting Materials, *Chem. Mater.*, 2014, **26**, 594-603.

20 J. Mei and Z. Bao: Side Chain Engineering in Solution-Processable Conjugated Polymers, *Chem. Mater.*, 2014, **26**, 604-615.

21 Z. Wu, X. Li, J. Li, H. Ågren, J. Hua and H. Tian: Effect of bridging group configuration on photophysical and photovoltaic performance in dye-sensitized solar cells, *J. Mater. Chem. A*, 2015, **3**, 14325-14333.

22 N. T. Shewmon, D. L. Watkins, J. F. Galindo, R. B. Zerdan, J. Chen, J. Keum, A. E. Roitberg, J. Xue and R. K. Castellano: Enhancement in Organic Photovoltaic Efficiency through the Synergistic Interplay of Molecular Donor Hydrogen Bonding and π-Stacking, *Adv. Funct. Mater.*, 2015, **25**, 5166-5177.

23 G. L. Eakins, R. Pandey, J. P. Wojciechowski, H. Y. Zheng, J. E. A. Webb, C. Valéry, P. Thordarson, N. O. V. Plank, J. A. Gerrard and J. M. Hodgkiss: Functional Organic Semiconductors Assembled via Natural Aggregating Peptides, *Adv. Funct. Mater.*, 2015, **25**, 5640-5649.

24 T. Aytun, L. Barreda, A. Ruiz-Carretero, J. A. Lehrman and S. I. Stupp: Improving Solar Cell Efficiency through Hydrogen Bonding: A Method for Tuning Active Layer Morphology, *Chem. Mater.*, 2015, **27**, 1201-1209.

25 T. L. Nguyen, S. Song, S.-J. Ko, H. Choi, J.-E. Jeong, T. Kim, S. Hwang, J. Y. Kim and H. Y. Woo: Benzodithiophene-thiophene-based photovoltaic polymers with different side-chains, *J. Polym. Sci., Part A: Polym. Chem.*,2015, **53**, 854-862.

26 R. Fitzner, E. Mena-Osteritz, K. Walzer, M. Pfeiffer and P. Bäuerle: A–D–A-Type Oligothiophenes for Small Molecule Organic Solar Cells: Extending the π-System by Introduction of Ring-Locked Double Bonds, *Adv. Funct. Mater.*, 2015, **25**, 1845-1856.

27 B. M. Schulze, N. T. Shewmon, J. Zhang, D. L. Watkins, J. P. Mudrick, W. Cao, R. Bou Zerdan, A. J. Quartararo, I. Ghiviriga, J. Xue and R. K. Castellano: Consequences of hydrogen bonding on molecular organization and charge transport in molecular organic photovoltaic materials, *J. Mater. Chem. A*, 2014, **2**, 1541-1549.

28 A. Petersen, A. Ojala, T. Kirchartz, T. A. Wagner, F. Würthner and U. Rau: Field-dependent exciton dissociation in organic heterojunction solar cells, *Phys. Rev. B*, 2012, **85**, 245208.

29 H. Bürckstümmer, E. V. Tulyakova, M. Deppisch, M. R. Lenze, N. M. Kronenberg, M. Gsänger, M. Stolte, K. Meerholz and F. Würthner: Efficient Solution-Processed Bulk Heterojunction Solar Cells by Antiparallel Supramolecular Arrangement of Dipolar Donor–Acceptor Dyes, *Angew. Chem. Int. Ed.*, 2011, **123**, 11832-11836.

30 F. Würthner, Z. J. Chen, F. J. M. Hoeben, P. Osswald, C. C. You, P. Jonkheijm, J. von Herrikhuyzen, A. Schenning, P. van der Schoot, E. W. Meijer, E. H. A. Beckers, S. C. J. Meskers and R. A. J. Janssen: Supramolecular p−n-Heterojunctions by Co-Self-Organization of Oligo(*p*-phenylene Vinylene) and Perylene Bisimide Dyes, *J. Am. Chem. Soc.*, 2004, **126**, 10611-10618.

31 F. Würthner and S. Yao: Dipolar dye aggregates: a problem for nonlinear optics, but a chance for supramolecular chemistry, *Angew. Chem. Int. Ed.*, 2000, **39**, 1978-1981.

32 M. Presselt, F. Herrmann, S. Shokhovets, H. Hoppe, E. Runge and G. Gobsch: Sub-bandgap absorption in polymer-fullerene solar cells studied by temperature-dependent external quantum efficiency and absorption spectroscopy, *Chem. Phys. Lett.*, 2012, **542**, 70-73.

33 M. Presselt, F. Herrmann, H. Hoppe, S. Shokhovets, E. Runge and G. Gobsch: Influence of Phonon Scattering on Exciton and Charge Diffusion in Polymer-Fullerene Solar Cells, *Adv. Energy Mater.*, 2012, **2**, 999-1003.

34 M. P. Ouattara, S. Lenfant, D. Vuillaume, M. Pezolet, J.-F. Rioux-Dube, J. Brisson and M. Leclerc: Langmuir–Blodgett Films of Amphiphilic Thieno[3,4-*c*]pyrrole-4,6-dione-Based Alternating Copolymers, *Macromolecules*, 2013, **46**, 6408-6418.

35 A. Lodi, F. Momicchioli, M. Caselli, G. Giancane and G. Ponterini: A comparative study of two amphiphilic merocyanines: from monomers to aggregates in Langmuir and Langmuir–Blodgett mixed films, *RSC Adv.*, 2013, **3**, 1468-1475.

36 D. Bauman, R. Hertmanowski, K. Stefańska and R. Stolarski: The synthesis of novel perylene-like dyes and their aggregation properties in Langmuir and Langmuir–Blodgett films, *Dyes Pigm.*, 2011, **91**, 474-480.

37 Y. Yajie, J. Yadong, X. Jianhua and Y. Junsheng: Self-assembly of conducting polymer nanowires as hole injection layer for organic light-emitting diodes applications, *Proc. SPIE - Int. Soc. Opt. Eng.*, 2010, **7658**, 76583I.

38 K. Ikegami: Dye aggregates formed in Langmuir–Blodgett films of amphiphilic merocyanine dyes, *Curr. Appl Phys.*, 2006, **6**, 813-819.

39 P. A. Antunes, C. J. L. Constantino, R. F. Aroca and J. Duff: Langmuir and Langmuir–Blodgett Films of Perylene Tetracarboxylic Derivatives with Varying Alkyl Chain Length: Film Packing and Surface-Enhanced Fluorescence Studies, *Langmuir*, 2001, **17**, 2958-2964.

40 F. Herrmann, B. Muhsin, C. R. Singh, S. Shokhovets, G. Gobsch, H. Hoppe and M. Presselt: Influence of Interface Doping on Charge-Carrier Mobilities and Sub-Bandgap Absorption in Organic Solar Cells, *J. Phys. Chem. C*, 2015, **119**, 9036-9040.

41 A. S. Weingarten, R. V. Kazantsev, L. C. Palmer, M. McClendon, A. R. Koltonow, P. S. SamuelAmanda, D. J. Kiebala, M. R. Wasielewski and S. I. Stupp: Self-assembling hydrogel scaffolds for photocatalytic hydrogen production, *Nat Chem*, 2014, **6**, 964-970.

42 H. Shi, N. Zhao, D. Ding, J. Liang, B. Z. Tang and B. Liu: Fluorescent light-up probe with aggregation-induced emission characteristics for in vivo imaging of cell apoptosis, *Org. Biomol. Chem.*, 2013, **11**, 7289-7296.

43 A. Di Fiore, S. M. Monti, A. Innocenti, J.-Y. Winum, G. De Simone and C. T. Supuran: Carbonic anhydrase inhibitors: Crystallographic and solution binding studies for the interaction of a boron-containing aromatic sulfamide with mammalian isoforms I–XV, *Bioorg. Med. Chem. Lett.*, 2010, **20**, 3601-3605.

44 A. K. Gadad, C. S. Mahajanshetti, S. Nimbalkar and A. Raichurkar: Synthesis and antibacterial activity of some 5-guanylhydrazone/thiocyanato-6-arylimidazo[2,1-b]-1,3,4-

thiadiazole-2-sulfonamide derivatives, *Eur. J. Med. Chem.*, 2000, **35**, 853-857.
45 Z. Chen, W. Xu, K. Liu, S. Yang, H. Fan, P. S. Bhadury, D. Y. Hu and Y. Zhang: Synthesis and Antiviral Activity of 5-(4-Chlorophenyl)-1,3,4-Thiadiazole Sulfonamides, *Molecules*, 2010, **15**, 9046-9056.
46 I. R. Ezabadi, C. Camoutsis, P. Zoumpoulakis, A. Geronikaki, M. Soković, J. Glamočilija and A. Ćirić: Sulfonamide-1,2,4-triazole derivatives as antifungal and antibacterial agents: Synthesis, biological evaluation, lipophilicity, and conformational studies, *Bioorg. Med. Chem.*, 2008, **16**, 1150-1161.
47 S. M. Sondhi, M. Johar, N. Singhal, S. G. Dastidar, R. Shukla and R. Raghubir: Synthesis and Anticancer, Antiinflammatory,and Analgesic Activity Evaluation of Some Sulfa Drug and Acridine Derivatives, *Monatsh. Chem.*, 2000, **131**, 511-520.
48 E. Täuscher, D. Weiß, R. Beckert and H. Görls: Synthesis and Characterizationof New 4-Hydroxy-1, 3-thiazoles, *Synthesis*, 2010, 1603-1608.
49 J. S. de Melo, L. S. M. Silva, L. S. G. Arnaut and R. S. Becker: Singlet and triplet energies of a-oligothiophenes: A spectroscopic, theoretical, and photoacoustic study: Extrapolation to polythiophene, *J. Chem. Phys.*, 1999, **111**, 5427-5433.
50 D. G. Patel, F. Feng, Y.-y. Ohnishi, K. A. Abboud, S. Hirata, K. S. Schanze and J. R. Reynolds, *Journal of the American Chemical Society*, 2012, **134**, 2599-2612.
51 Z. Zhou, T. S. Corbitt, A. Parthasarathy, Y. Tang, L. K. Ista, K. S. Schanze and D. G. Whitten: "End-Only" Functionalized Oligo(phenylene ethynylene)s: Synthesis, Photophysical and Biocidal Activity, *J. Phys. Chem. Lett.*, 2010, **1**, 3207-3212.
52 C. A. Hunter and J. K. M. Sanders: The nature of π–π interactions, *J. Am. Chem. Soc.*, 1990, **112**, 5525-5534.
53 E. A. Meyer, R. K. Castellano and F. Diederich: Interactions with aromatic rings in chemical and biological recognition, *Angew. Chem. Int. Ed.*, 2003, **42**, 1210-1250.
54 C. D. Sherrill: Energy Component Analysis of π Interactions, *Acc. Chem. Res.*, 2013, **46**, 1020-1028.
55 G. Chessari, C. A. Hunter, C. M. R. Low, M. J. Packer, J. G. Vinter and C. Zonta: An Evaluation of Force-Field Treatments of Aromatic Interactions, *Chem. Eur. J.*, 2002, **8**, 2860-2867.
56 J. Tomasi, B. Mennucci and R. Cammi: Quantum mechanical continuum solvation models, *Chem. Rev.*, 2005, **105**, 2999-3093.
57 M. J. Frisch, G. W. Trucks, H. B. Schlegel, G. E. Scuseria, M. A. Robb, J. R. Cheeseman, G. Scalmani, V. Barone, B. Mennucci, G. A. Petersson, H. Nakatsuji, M. Caricato, X. Li, H. P. Hratchian, A. F. Izmaylov, J. Bloino, G. Zheng, J. L. Sonnenberg, M. Hada, M. Ehara, K. Toyota, R. Fukuda, J. Hasegawa, M. Ishida, T. Nakajima, Y. Honda, O. Kitao, H. Nakai, T. Vreven, J. A. Montgomery Jr., J. E. Peralta, F. Ogliaro, M. Bearpark, J. J. Heyd, E. Brothers, K. N. Kudin, V. N. Staroverov, R. Kobayashi, J. Normand, K. Raghavachari, A. Rendell, J. C. Burant, S. S. Iyengar, J. Tomasi, M. Cossi, N. Rega, M. J. Millam, M. Klene, J. E. Knox, J. B. Cross, V. Bakken, C. Adamo, J. Jaramillo, R. Gomperts, R. E. Stratmann, O. Yazyev, A. J. Austin, R. Cammi, C. Pomelli, J. W. Ochterski, R. L. Martin, K. Morokuma, V. G. Zakrzewski, G. A. Voth, P. Salvador, J. J. Dannenberg, S. Dapprich, A. D. Daniels,Ö. Farkas, J. B. Foresman, J. V. Ortiz, J. Cioslowski, D. J. Fox,. *Gaussian 09, Revision A.02*; Gaussian, Inc.: Wallingford, CT, USA, 2009.
58 D. Jacquemin, E. Perpète, I. Ciofini, C. Adamo, Assessment of the ωB97 family for excited-state calculations, *Theor Chem Acc.*, 2011, **128**, 127-136.
59 D. Jacquemin, V. Wathelet, E. A. Perpète, C. Adamo, *J. Chem. Theory Comput.*, Extensive TD-DFT Benchmark: Singlet-Excited States of Organic Molecules, 2009, **5**, 2420-2435.
60 L. Pinto da Silva, J. C. G. Esteves da Silva, Analysis of the performance of DFT functionals in the study of light emission by oxyluciferin analogs, *Int. J. Quantum Chem.*, 2013, **113**, 45-51.
61 P. Dynarowicz-Łątka, A. Dhanabalan and O. N. Oliveira Jr.: Modern physicochemical research on Langmuir monolayers, *Adv. Colloid Interface Sci.*, 2001, **91**, 221-293.
62 J. Jin, L. S. Li, Y. Li, Y. J. Zhang, X. Chen, D. Wang, S. Jiang, T. J. Li, L. B. Gan and C. H. Huang: Structural Characterizations of C_{60}-Derivative Langmuir–Blodgett Films and Their Photovoltaic Behaviors, *Langmuir*, 1999, **15**, 4565-4569.
63 C. Roldan-Carmona, C. Rubia-Paya, M. Perez-Morales, M. T. Martin-Romero, J. J. Giner-Casares and L. Camacho: UV-Vis reflection spectroscopy under variable angle incidence at the air–liquid interface, *Phys. Chem. Chem. Phys.*, 2014, **16**, 4012-4022.
64 G. Zhavnerko and G. Marletta: Developing Langmuir–Blodgett strategies towards practical devices, *Mater. Sci. Eng., B*, 2010, **169**, 43-48.
65 K. Ekelund, E. Sparr, J. Engblom, H. Wennerström and S. Engström: An AFM Study of Lipid Monolayers. 1. Pressure-Induced Phase Behavior of Single and Mixed Fatty Acids, *Langmuir*, 1999, **15**, 6946-6949.
66 T. A. Halgren: Merck molecular force field. I. Basis, form, scope, parameterization, and performance of MMFF94, *J. Comput. Chem.*, 1996, **17**, 490-519.
67 K. Ariga, Y. Yamauchi, T. Mori and J. P. Hill: 25th Anniversary Article: What Can Be Done with the Langmuir-Blodgett Method? Recent Developments and its Critical Role in Materials Science, *Adv. Mater.*, 2013, **25**, 6477-6512.
68 M. Van der Auweraer, B. Verschuere and F. C. De Schryver: Absorption and fluorescence properties of Rhodamine B derivatives forming Langmuir-Blodgett films, *Langmuir*, 1988, **4**, 583-588.
69 U. Rösch, S. Yao, R. Wortmann and F. Würthner: Fluorescent H-Aggregates of Merocyanine Dyes, *Angew. Chem. Int. Ed.*, 2006, **45**, 7026-7030.
70 R. F. Chen and J. R. Knutson: Mechanism of fluorescence concentration quenching of carboxyfluorescein in liposomes: Energy transfer to nonfluorescent dimers, *Anal. Biochem.*, 1988, **172**, 61-77.
71 E. A. Margulies, L. E. Shoer, S. W. Eaton and M. R. Wasielewski: Excimer formation in cofacial and slip-stacked perylene-3,4:9,10-bis(dicarboximide) dimers on a redox-inactive triptycene scaffold, *Phys. Chem. Chem. Phys.*, 2014, **16**, 23735-23742.
72 H. Yoo, J. Yang, A. Yousef, M. R. Wasielewski and D. Kim: Excimer Formation Dynamics of Intramolecular π-Stacked Perylenediimides Probed by Single-Molecule Fluorescence Spectroscopy, *J. Am. Chem. Soc.*, 2010, **132**, 3939-3944.
73 J. M. Giaimo, J. V. Lockard, L. E. Sinks, A. M. Scott, T. M. Wilson and M. R. Wasielewski: Excited Singlet States of Covalently Bound, Cofacial Dimers and Trimers of Perylene-3,4:9,10-bis(dicarboximide)s, *J. Phys. Chem. A*, 2008, **112**, 2322-2330.
74 M. I. Sluch, A. G. Vitukhnovsky and M. C. Petty: Pyrene excimer formation in Langmuir-Blodgett films, *Thin Solid Films*, 1996, **284–285**, 622-626.
75 P. Debnath, S. Chakraborty, S. Deb, J. Nath, D. Bhattacharjee and S. A. Hussain: Reversible Transition between Excimer and J-Aggregate of Indocarbocyanine Dye in Langmuir–Blodgett (LB) Films, *J. Phys. Chem. C*, 2015, **119**, 9429-9441.
76 L. Lu, R. J. Lachicotte, T. L. Penner, J. Perlstein and D. G. Whitten: Exciton and Charge-Transfer Interactions in Nonconjugated Merocyanine Dye Dimers: Novel

Solvatochromic Behavior for Tethered Bichromophores and Excimers, *J. Am. Chem. Soc.*, 1999, **121**, 8146-8156.
77 M. Montalti, A. Credi, L. Prodi and M. T. Gandolfi, *Handbook of Photochemistry*, 3rd edition, Taylor & Francis, Boca Raton, 2006.
78 K. Suzuki, A. Kobayashi, S. Kaneko, K. Takehira, T. Yoshihara, H. Ishida, Y. Shiina, S. Oishic and S. Tobita, Reevaluation of absolute luminescence quantum yields of standard solutions using a spectrometer with an integrating sphere and a back-thinned CCD detector, *Phys. Chem. Chem. Phys.*, 2009, **11**, 9850-9860.
79 A. M. Brouwer, Standards for photoluminescence quantum yield measurements in solution (IUPAC Technical Report), *Pure Appl. Chem.*, 2011, **83**, 2213-2228.
80 R. Ditchfield, W. J. Hehre and J. A. Pople: Self-Consistent Molecular-Orbital Methods. IX. An Extended Gaussian-Type Basis for Molecular-Orbital Studies of Organic Molecules, *J. Chem. Phys.*, 1971, **54**, 724-728.
81 T. Yanai, D. P. Tew, N. C. Handy, A new hybrid exchange–correlation functional using the Coulomb-attenuating method (CAM-B3LYP), *Chem. Phys. Lett.*, 2004, **393**, 51-57.
82 M. Kasha, Characterization of Electronic Transitions in Complex Molecules, *Discuss. Faraday Soc.*, 1950, **9**, 14-19.
83 B. V. Nonius., *COLLECT*, Data Collection Software, Netherlands, 1998.
84 Z. Otwinowski and W. Minor: "Processing of X-Ray Diffraction Data Collected in Oscillation Mode" in *Methods in Enzymology*, Vol. 276, Macromolecular Crystallography, Part A, edited by C.W. Carter and R.M. Sweet, 307-326, Academic Press, San Diego, CA, USA, 1997.
85 *SADABS 2.10*, Bruker-AXS Inc., 2002, Madison, WI, USA.
86 G. M. Sheldrick: A short history of SHELX, *Acta Cryst.*, 2008, **A46**, 112-122.

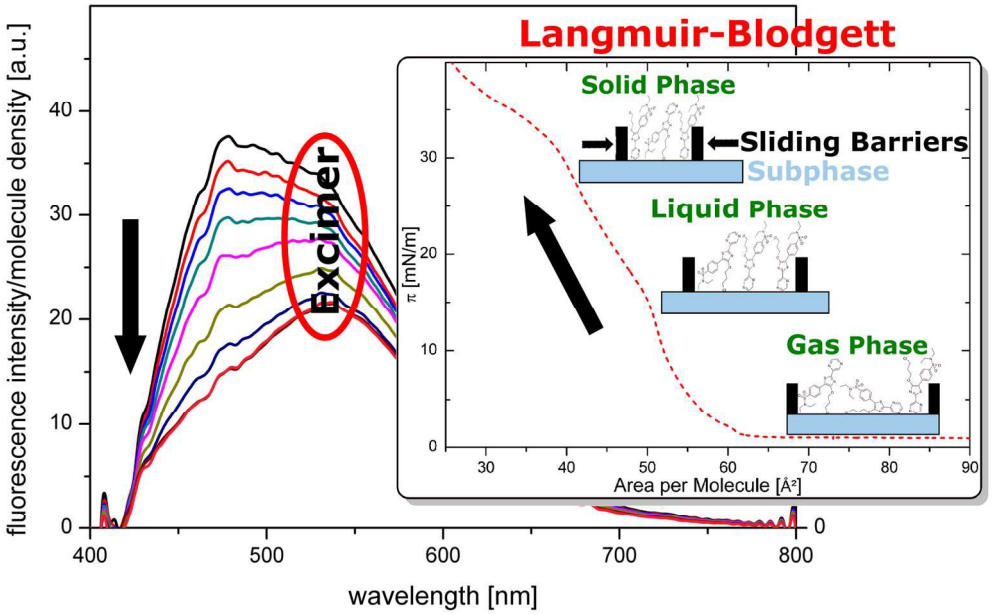

Processing of 4-alkoxythiazole sulfonamides via Langmuir-Blodgett technique gave an insight into the influence of aggregation on the electro optical properties of thin films.